Heliyon 8 (2022) e11358

Contents lists available at ScienceDirect

Heliyon

journal homepage: www.cell.com/heliyon

Research article

Circularly polarized luminescence of pinene-modified tetradentate platinum(II) enantiomers containing fused 5/6/6 metallocycles

Hua-Hong Zhang [a], Jing Jing [a], Guo Xu [a], Yi-Xin Song [a], Shui-Xing Wu [a], Xing-Han Chen [b], Da-Shuai Zhang [a], Xiao-Peng Zhang [a,*], Zai-Feng Shi [a]

[a] College of Chemistry and Chemical Engineering, Key Laboratory of Water Pollution Treatment & Resource Reuse of Hainan Province, Hainan Normal University, Haikou 571158, PR China

[b] Jiangsu Co-Innovation Center of Efficient Processing and Utilization of Forest Resources, College of Chemical Engineering, Nanjing Forestry University, Nanjing, 210037, PR China

ARTICLE INFO

Keywords:
Circularly polarized luminescence
Tetradentate platinum(II) complex
Pinene
Fused metallocycles
Aggregation-induced emission enhancement

ABSTRACT

In this study, a couple of tetradentate Pt(II) enantiomers ((−)-**1** and (+)-**1**) and a couple of tetradentate Pt(IV) enantiomers ((−)-**2** and (+)-**2**) containing fused 5/6/6 metallocycles have been synthesized by controlling reaction conditions. Two valence forms could transform into each other through mild chemical oxidants and reductants. Single-crystal X-ray diffraction confirms the structures of (−)-1 and (−)-2. The coordination sphere of the Pt(II) cation in (−)-**1** displays a distorted square-planar geometry and a platinum centroid helix chirality. In contrast, the structure of (−)-**2** reveals a distorted octahedral geometry. The solution and the solid of (−)-**1** are highly luminescent. Complex (−)-**1** shows a prominent aggregation-induced emission enhancement (AIEE) behavior in DMSO/water solution with emission quantum yield (Φ_{em}) up to 73.2%. Furthermore, highly phosphorescent Pt(II) enantiomers exhibit significant circularly polarized luminescence (CPL) with a dissymmetry factor (g_{lum}) of order 10^{-3} in CH_2Cl_2 solutions at room temperature. Symmetrically appreciable CPL signals are observed for the enantiomers (−)-**1** and (+)-**1**.

1. Introduction

Circularly polarized luminescent (CPL) Pt(II) complexes have garnered increasing interest due to their tunable emission wavelengths and high emission quantum yields (Φ_{em}), showing promising potential in circularly polarized phosphorescent organic light-emitting diodes (CP-PhOLEDs) [1, 2, 3, 4, 5]. Several strategies have been adopted to develop CPL phosphorescent Pt(II) complexes. Initially, intrinsic CPL-active chiral π-systems such as helicene [6, 7, 8] and binaphthyl derivatives [9, 10] have been decorated on the parent phosphorescent Pt(II) skeletons. Furthermore, square-planar Pt(II) complexes prefer to assemble into supramolecular helical aggregates, exhibiting chiroptically active ^{3}MMLCT signals [11, 12, 13, 14, 15, 16, 17, 18, 19]. In addition to the above two strategies, another method to obtain CPL-active Pt(II) complexes is to utilize coordination chirality [20, 21, 22, 23]. Through choosing appropriate chelating ligands such as *trans*-spanning phenylpyridine, substituted (2-thienyl)pyridine and *trans*-bis[(β-iminomethyl)aryloxy], chiral-at-metal, chiral-at-plane and chiral-at-cluster Pt(II) complexes with significant CPL response and distinct anisotropic factors g_{lum} ($g_{lum} = 2\Delta I/I = 2(I_L–I_R)/(I_L + I_R)$, where I_L and I_R refer, respectively, to the intensity of circularly polarized emissions of left and right) could be successfully induced [24, 25, 26, 27, 28, 29]. When these twisted Pt(II) complexes serve as chiral emitters, low-cost CP-PhOLEDs could be fabricated through a solution process, achieving competitive luminance efficiency, external quantum efficiency, and asymmetry factor [30, 31].

Tetradentate Pt(II) complexes feature high thermal stabilities and emission quantum yields with Φ_{em} values of up to 100% so that they can serve as efficient phosphorescent emitters with high color purity for full-color display OLED applications [32, 33, 34, 35, 36, 37]. The emission colors of the tetradentate Pt(II) complexes could be tuned in the entire visible region by changing the heteroaromatic rings [38, 39, 40]. Six-membered metallocycles occupy more angular space, rendering the tetradentate complex non-planar [41]. Tetradentate Pt(II) complexes containing fused 5/6/6 or 6/6/6 metallocycles exhibit a more significant degree of distortions with bigger dihedrals than those with fused 5/6/5 or 5/5/6 metallocycles [42, 43, 44]. Hence, the molecular geometry of tetradentate Pt(II) complexes with more six-membered-ring chelates would be more distorted, which is beneficial for alleviating

* Corresponding author.
E-mail address: zxp_inorganic@126.com (X.-P. Zhang).

https://doi.org/10.1016/j.heliyon.2022.e11358
Received 25 September 2022; Received in revised form 12 October 2022; Accepted 27 October 2022

intermolecular Pt···Pt interactions. The blue or green luminescence of tetradentate Pt(II) complexes containing fused 5/6/6 or 6/6/6 metallocycles originates mainly from the monomeric ligand-centered triplet transition state (^{3}LC), and excimeric emission is scarcely found [45, 46]. On the contrary, the planar complexes with fused 5/6/5 or 5/5/6 metallocycles are apt to form excimers; therefore, it is possible to regulate emission from narrow blue to broad white by managing monomeric and excimeric states [47, 48, 49].

Tetradentate Pt(II) complexes containing fused 5/6/6 or 6/6/6 metallocycles are significantly distorted, and their terminal fragments deviate from the coordinating plane [41, 42, 43, 44]. Therefore, those twisted complexes may possess interesting chiral optical properties. Recently, Zheng et al. developed a series of tetradentate Pt(II) complexes containing fused 5/6/6 or 6/6/6 metallocycles, demonstrating apparent circularly polarized luminescence (CPL) properties and exhibiting good device performances in CP-PhOLEDs [31]. However, the separation of the enantiomers from racemates through chiral resolution is complicated, and racemization may occur at room temperature. Subsequently, employing (RR)/(SS)-1,2-diphenylethane-1,2-diamine as the intrinsic chiral source, Zheng et al. designed and synthesized two pairs of CPL-active Pt(II) complexes with fused 5/5/5 metallocycles, avoiding further chiral separation and possible racemization [28]. We have previously studied the CPL properties of pinene-containing cyclometalated Pt(II) complexes with chiral-at-metal and helical chirality [50, 51, 52, 53]. Pinenes with defined carbon stereocenters would control the specific configuration and stacking of Pt(II) complexes [50, 51, 52, 53, 54, 55]. In this work, a couple of pinene-functionalized phosphorescent tetradentate Pt(II) complexes ((−)-**1** and (+)-**1**) with fused 5/6/6 metallocycles have been prepared under the protection of argon (Scheme 1). Similarly to the reported results, a couple of novel enantiomeric tetradentate Pt(IV) complexes ((−)-**2** and (+)-**2**) were successfully isolated under-reacting in the air. The phosphorescent tetradentate Pt(II) complex (−)-**1** displays distinct AIEE behaviors. Significantly, the enantiomers (−)-**1** and (+)-**1** show clear and symmetric CPL activities with $|g_{lum}|$ of 10^{-3}.

2. Experimental section

2.1. General methods

All reagents were purchased from commercial suppliers and used as received. High-resolution ESI (HR-ESI) mass spectrometry spectra were acquired on a Thermo Scientific Q Exactive Mass Spectrometer. Elemental analysis was performed on a PerkinElmer 240C analyzer. The samples were dried under vacuum at 50 °C for 24 h to remove solvated molecules prior to elemental analysis. The ^{1}H and ^{13}C NMR spectra were obtained on a Bruker DRX-400 spectrometer. Coupling constants are given in hertz. UV-vis spectra were measured on a UV-3600 spectrophotometer. Photoluminescence (PL) spectra were measured with the Hitachi F-4600 PL spectrophotometer (λ_{ex} = 420 nm). Circular dichroism (CD) spectra in CH_2Cl_2 solution were recorded on a Jasco J-810 spectropolarimeter at a scan rate of 100 nm min^{-1} and a resolution of 1 nm at room temperature. CPL spectra were recorded using a circularly polarizer on a Jasco CPL-300 spectrophotometer at a scan rate of 100 nm min^{-1} and a resolution of 1 nm at room temperature.

2.2. Synthetic procedures

Synthesis of (−)-L. A 15 mL DMSO (pretreated with molecular sieve) solution of 394 mg (−)-4,5-pinene-3-bromophenyl-pyridine (1.2 mmol, 1.2 eq) and 187 mg 3-(pyridin-2-yloxy)phenol (1.0 mmol, 1.0 eq) was added into a 25 mL Schlenk flask containing anhydrous potassium phosphate (2.1 eq), CuI (0.10 eq) and 2-picolinic acid (0.20 eq). The solution was refluxed at 120 °C under dark in an argon atmosphere for three days. The solution was cooled to room temperature and extracted

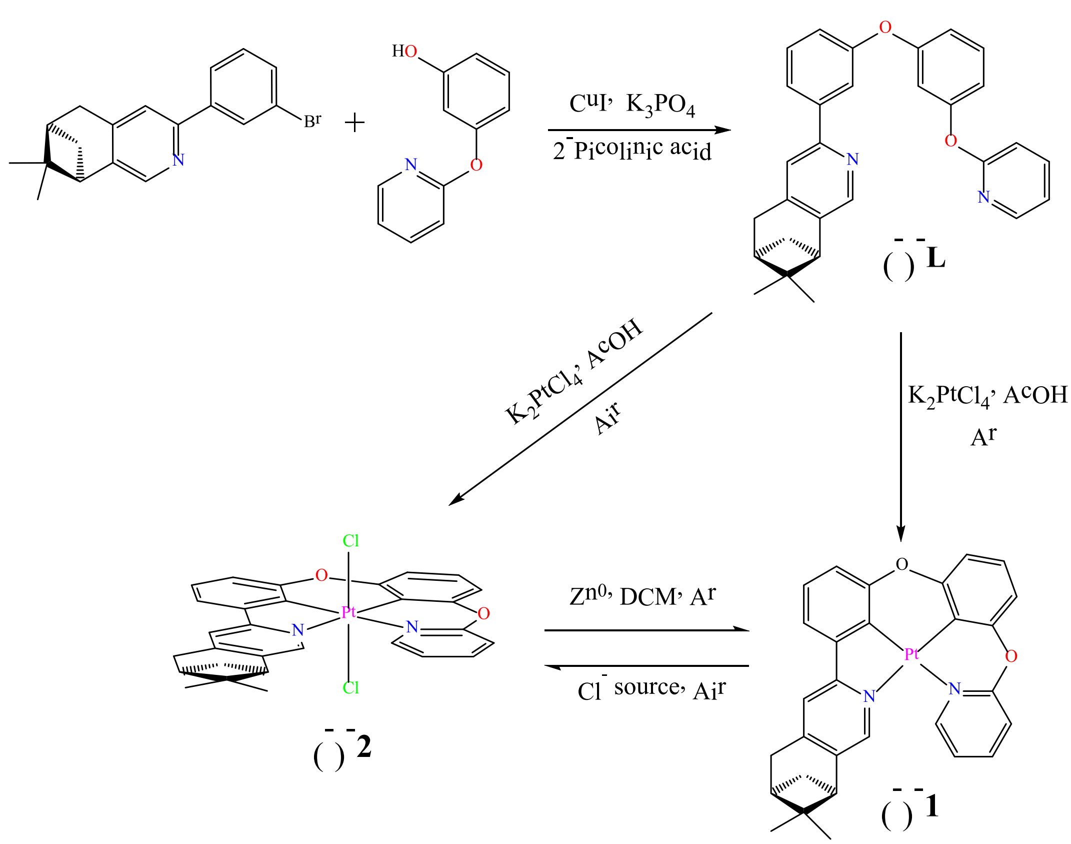

Scheme 1. Synthesis route of (−)-**1** and (−)-**2**.

with CH_2Cl_2 3 times. The organic layers were combined and dried over Na_2SO_4. The crude product was purified by silica gel flash chromatography with an eluent of PE: EA = 5 : 1. ^{1}H NMR (400 MHz, CD_2Cl_2-d_2, RT): δ 8.33 [s, 1H], 8.25 [d, J = 3.2 Hz, 1H], 7.94 [s, 1H], 7.92[d, J = 8.0 Hz, 1H], 7.72 [t, J = 7.2 Hz, 1H], 7.64 [s, 1H], 7.54 [t, J = 8.0 Hz, 1H], 7.44 [t, J = 8.0 Hz, 1H], 7.23 [d, J = 7.6 Hz, 1H], 7.00–7.06 [m, 5H], 3.08 [s, 2H], 2.93 [t, J = 5.2 Hz, 1H], 2.75–2.81 [m, 1H], 2.37 [m, 1H], 1.50 [s, 3H], 1.30 [d, J = 9.6 Hz, 1H], 0.75 [s, 3H]. ^{13}C NMR (100 MHz, CD_2Cl_2-d2, RT): δ 163.5, 158.8, 157.2, 155.7, 154.4, 147.6, 146.0, 145.3, 142.0, 141.8, 139.6, 130.4, 130.2, 122.1, 120.0, 119.5, 118.9, 117.7, 116.0, 114.5, 111.9, 111.8, 44.5, 40.3, 39.3, 32.9, 32.0, 26.0, 21.4. HR-MS (ESI) (m/z) $[M + H]^+$ calcd for $C_{29}H_{27}N_2O_2^+$, 435.2067; found, 435.2231. Anal. Calcd for $C_{29}H_{26}N_2O_2$: C, 80.16; H, 6.03; N, 6.45%. Found: C, 80.18; H, 6.01; N, 6.47%.

Synthesis of (−)-1. A 50 mL eggplant-shaped bottle was charged with (−)-L (434 mg, 1 mmol), K_2PtCl_4 (415 mg, 1 mmol) and tetrabutylammonium bromide (644 mg, 2 mmol) in AcOH (25 mL) at 77 K and was degassed and refilled with argon three times. The reaction mixture was refluxed at 115 °C for three days under argon. After the reaction finished, the residue was filtered and washed with water. The crude product was purified by silica gel flash chromatography with an eluent of CH_2Cl_2. A green-yellow powder was obtained finally. ^{1}H NMR (400 MHz, CD_2Cl_2-d_2, RT): δ 8.55 [dd, J_1 = 5.2 Hz, J_2 = 1.6 Hz, 1H], 7.91 [m, 2H], 7.67 [s, 1H], 7.39 [d, J = 7.6 Hz, 1H], 7.32 [d, J = 8.4 Hz, 1H], 7.17 [d, J = 6.4 Hz, 1H], 7.11 [d, J = 7.6 Hz, 1H], 6.97–7.03 [m, 2H], 6.93–6.96 [tt, J_1 = 8.0 Hz, J_2 = 1.6 Hz, 1H], 6.84 [dd, J_1 = 7.6 Hz, J_2 = 1.2 Hz, 1H], 3.03 [d, J = 2.4 Hz, 2H], 2.73 [t, J = 5.6 Hz, 1H], 2.64–2.70 [m, 1H], 2.27 [m, 1H], 1.34 [s, 3H], 1.21 [d, J = 9.6 Hz, 1H], 0.62 [s, 3H]. ^{13}C NMR (100 MHz, CD_2Cl_2-d_2, RT): δ 163.2, 160.5, 156.0, 154.3, 152.4, 148.5, 148.0, 147.7, 143.2, 142.5, 140.4, 124.6, 124.3, 120.4, 119.3, 117.7, 116.9, 116.0, 112.6, 109.7, 105.6, 44.7, 39.9, 39.4, 33.2, 31.7, 25.6, 21.2. HR-MS (ESI) (m/z) $[M + H]^+$ calcd for $C_{29}H_{25}N_2O_2Pt^+$, 628.1564; found, 628.1542. Anal. Calcd for $C_{29}H_{24}N_2O_2Pt$: C, 55.50; H, 3.85; N, 4.46%. Found: C, 55.53; H, 3.86; N, 4.45%.

Synthesis of (−)-2. A mixture of (−)-L (434 mg, 1 mmol), K_2PtCl_4 (415 mg, 1 mmol) and tetrabutylammonium bromide (644 mg, 2 mmol) in AcOH (25 mL) was allowed to reflux at 115 °C for three days under air. After the reaction finished, the residue was filtered and washed with water. The crude product was purified by silica gel flash chromatography with a CH_2Cl_2 eluent. A pale-yellow powder was obtained. ^{1}H NMR (400 MHz, CD_2Cl_2-d_2, RT): δ 8.74–8.86 [m, 1H], 8.14 [s, 1H], 8.00 [t, J = 4.0 Hz, 1H], 7.86 [s, 1H], 7.54 [d, J = 8.0 Hz, 1H], 7.36–7.41 [m, 2H], 7.17–7.25 [m, 1H], 7.05–7.13 [m, 2H], 6.99–7.00 [m, 1H], 6.91 [d, J = 8.0 Hz, 1H], 3,16 [s, 2H], 2.84 [t, J = 4.0 Hz, 1H], 2.67–2.73 [m, 1H], 2.30 [m, 1H], 1.36 [s, 3H], 1.23 [d, J = 8.0 Hz, 1H], 0.64 [s, 3H]. ^{13}C NMR (100 MHz, CD_2Cl_2-d_2, RT): δ 161.0, 159.1, 152.2, 151.9, 151.6, 149.9, 148.0, 147.5, 143.9, 143.5, 142.8, 142.2, 127.7, 127.3, 121.3, 121.0, 119.3, 119.2, 116.7, 115.1, 114.1, 112.7, 45.0, 39.8, 39.2, 33.1, 31.5, 25.5, 21.2. HR-MS (ESI) (m/z) $[M + Na]^+$ calcd for $C_{29}H_{24}Cl_2N_2NaO_2Pt^+$, 721.4863; found, 721.0714. Anal. Calcd for $C_{29}H_{24}Cl_2N_2O_2Pt$: C, 49.87; H, 3.46; N, 4.01%. Found: C, 49.88; H, 3.47; N, 4.00%.

Transformation from (−)-2 to (−)-1. Complex (−)-**2** can be successfully transformed to (−)-**1** by a heterogeneous reduction with Zn^0. Under an argon atmosphere, a mixture of (−)-**2** (698 mg, 1 mmol), activated Zn^0 dust (130 mg, 2 mmol) and 15 mL anhydrous CH_2Cl_2 in a 25 mL Schlenk flask was heated to 40 °C for 2 days. After cooling down, the solution was filtered through Celite and the filtrate was concentrated by rotary evaporation. The crude product was purified by silica gel flash chromatography eluting with CH_2Cl_2 to give (−)-**1** as a green-yellow solid.

Transformation from (−)-1 to (−)-2. Tetrabutyl ammonium chloride (834 mg, 3 mmol in 5 mL CH_2Cl_2) was added dropwise to a stirred CH_2Cl_2 solution of (−)-**1** (314 mg, 0.5 mmol). And the yellow solution was heated to 40 °C for 24 h in air. After the solvent was removed in vacuo, the pale-yellow powder (−)-**2** was washed with methanol.

2.3. Single crystal X-ray structure determination

Single-crystal X-ray diffraction measurements were performed on a Bruker SMART APEX CCD and Xcalibur Atlas Gemini ultra. Intensities were collected with graphite monochromatized Mo Kα radiation (λ = 0.71073 Å) or Ga Kα radiation (λ = 1.34139 Å) operating at 50 kV and 30 mA, using ω/2θ scan mode. The data reduction was made with the Bruker SAINT package [56]. Absorption corrections were performed using the SADABS program [57]. The structures were solved by direct methods and refined on F^2 by full-matrix least-squares using SHELXL-2018/3 (Sheldrick, 2018) with anisotropic displacement parameters for all non-hydrogen atoms in the two structures. Hydrogen atoms bonded to carbon atoms were placed in calculated positions and refined as riding mode, with C–H = 0.93 Å (methane) or 0.96 Å (methyl) and Uiso(H) = 1.2 Ueq ($C_{methane}$) or Uiso(H) = 1.5 Ueq (C_{methyl}). All computations were carried out using the SHELXL-2018/3 program package [58]. CCDC numbers 2206659–2206660 contain the supplementary crystallographic data for this paper. These data can be obtained free of charge from the Cambridge Crystallographic Data Centre via www.ccdc.cam.ac.uk/data_request/cif.

2.4. Calculation methods

The crystal structures of (−)-**1** and (−)-**2** were used as starting geometries, and calculations were performed with the Gaussian 09 program [59]. Geometry optimizations of ground states were simulated with density functional theory (DFT) at the hybrid functional PBE1PBE-D3/LANL2DZ (Pt) and PBE1PBE-D3/6-31g(d,p) (H, C, N, Cl) levels using CH_2Cl_2 as solvent. The solvent effect is based on the polarizable continuum model (PCM). The optimized structures of (−)-**1** and (−)-**2** were used to calculate the lowest singlet electronic transition using the time-dependent density functional theory (TDDFT) method. The geometry of the first triplet state (T_1) was optimized and the analysis of the natural transition orbital (NTO) was carried out for the excitation of $S_0 \rightarrow T_1$ [40,44-46]. Mulliken population analysis (MPA) was utilized to obtain the electron density distribution of each atom in the specific molecular orbital of the Pt(II) complexes using the Multiwfn program [60].

3. Results and discussion

3.1. Synthesis and characterization

The preparation of tetradentate Pt(II) complexes (−)-**1** and (−)-**2** is illustrated in Scheme 1. The tetradentate ligand consists of two moieties that one is phenyl-pyridine and another is phenoxyl-pyridine. An oxygen atom bridges the two segments mentioned above. Based on our familiar procedures, the precursor (−)-4,5-pinene-2-(5-bromophenyl) pyridine was prepared via the Kröhnke strategy [61]. The reactant 3-(pyridin-2-yloxy)phenol was synthesized according to reference [41]. A copper(I)-catalyzed C–O cross-coupling reaction of (−)-4,5-pinene-2-(5-bromophenyl) pyridine and 3-(pyridin-2-yloxy)phenol in the presence of K_3PO_4 give the tetradentate ligand (−)-L. Under strictly argon, tetradentate Pt(II) complex (−)-**1** was obtained by the direct metalation between (−)-L and K_2PtCl_4 in acetic acid media. Under the same conditions, tetradentate Pt(IV) complex (−)-**2** could be synthesized in the air. Two oxidation forms Pt(II)/(IV) remained stable in the solution and solid state, and the oxidation and reduction of the platinum center were reversible. The enantiomers (+)-**1** and (+)-**2** were also prepared through the same method. The structures of tetradentate Pt(II) and Pt(IV) complexes have been determined by X-ray diffraction, ^{1}H and ^{13}C NMR spectroscopy (Figures S1-S6), and high-resolution mass spectrometry (HRMS).

3.2. Crystal structures

Single crystals of (−)-**1** and (−)-**2** suitable for X-ray determination could be obtained. Through the slow evaporation in CH_2Cl_2/acetone (v/v = 1:1) solution at 0 °C, (−)-**1** crystallized as yellow blocks emitting green-yellow luminescence under UV radiation (λ = 365 nm). Non-emissive pale-yellow needles of (−)-**2** could be separated by the recrystallization in CH_2Cl_2/acetone (v/v = 1:1) solution at RT. Both complexes (−)-**1** and (−)-**2** crystallize in the same chiral space group, $P2_1$ of the monoclinic system, with two complex molecules per asymmetrical unit. The related crystallographic data are summarized in Table S1.

In the crystal structures of (−)-**1** and (−)-**2**, fused 5/6/6 metallocycles are expected to be formed after coordination (Figure 1). Metal-ligand Pt–C bond lengths range from 1.94 to 2.02 Å. In contrast, Pt–N coordinate bonds are slightly longer within 2.09–2.19 Å, demonstrating stronger Pt–C bonding interactions [40, 41, 42, 43, 44, 45, 46, 47, 48]. The coordination sphere of the Pt(II) cation in (−)-**1** displays a distorted square-planar geometry attributable to the boatlike conformation of two six-membered rings [40, 41, 42, 43]. The bite angles around Pt(II) center C1–Pt1–N2, C2–Pt1–N1, C3–Pt2–N4, and C4–Pt2–N3 (166.8–169.6°) significantly deviate from linearity. As revealed in Table 1, the dihedral angles between the terminal pyridine planes of two crystallographically independent molecules in (−)-**1** are 54.186° and 42.270°, affirming the intramolecular distortion and suggesting a platinum centroid helix chirality [28, 31].

The Pt nuclei in the crystal structure of (−)-**2** present an octahedral geometry with phenyl-pyridine and phenoxyl-pyridine moieties coordinating equatorially and two Cl^- occupying the axial positions (Figure 1) [62, 63]. Bite angles C1–Pt1–N2, C2–Pt1–N1, C3–Pt2–N4, and C4–Pt2–N3 (170.2–174.2°) in (−)-**2** are more linear relative to those angles of (−)-**1**, implying a slight distortion in octahedral geometry (Table 1). Given the twisted flexibility of the six-membered ring and steric hindrance of pinenes groups, intermolecular Pt···Pt and π–π interactions are not involved in the crystal packing of all crystal forms (Figure 1).

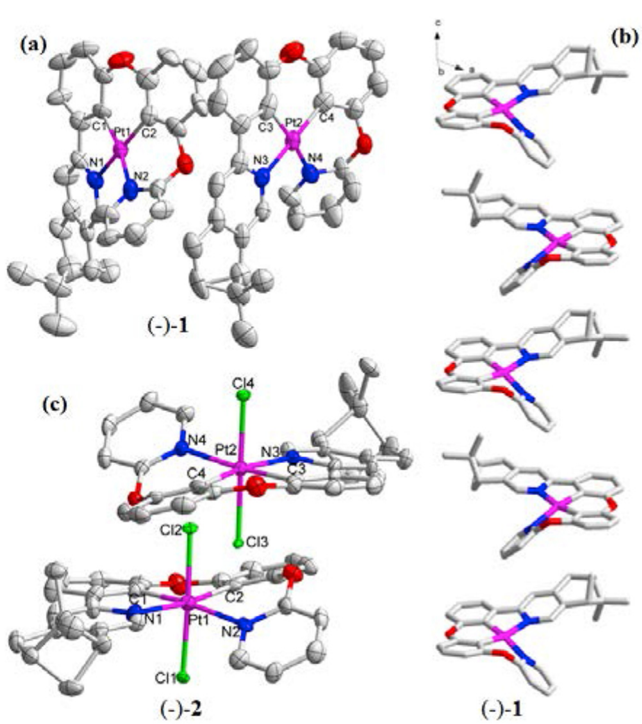

Figure 1. Crystal structure and crystal packing of (−)-**1** (a, b), and crystal structure of (−)-**2**.

Table 1. Molecular structures, selected bond lengths (Å), and angles (°) for (−)-**1** and (−)-**2**.

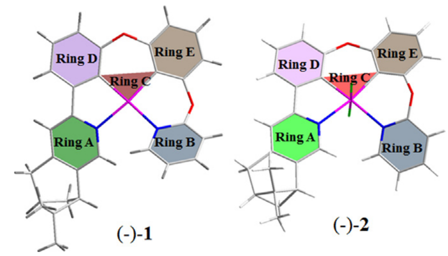

	(−)-1 y	(−)-2
Bond Length (Å)		
Pt1–C1	1.941(15)	1.992(12)
Pt1–C2	1.999(15)	2.016(12)
Pt1–N1	2.110(11)	2.153(10)
Pt1–N2	2.123(12)	2.191(11)
Pt2–C3	1.984(15)	1.993(11)
Pt2–C4	1.972(15)	2.009(12)
Pt2–N3	2.093(12)	2.160(10)
Pt2–N4	2.117(12)	2.181(10)
Bond Angle (°)		
C1–Pt1–C2	90.2(7)	92.1(5)
C1–Pt1–N1	80.9(6)	80.4(5)
C1–Pt1–N2	168.0(5)	173.1(4)
C2–Pt1–N1	166.9(5)	170.9(4)
C2–Pt1–N2	90.4(6)	87.8(4)
N1–Pt1–N2	100.4(5)	100.2(4)
C3–Pt2–C4	90.8(7)	92.2(5)
C3–Pt2–N3	81.7(6)	80.0(4)
C3–Pt2–N4	166.8(5)	174.2(4)
C4–Pt2–N3	169.6(5)	170.2(4)
C4–Pt2–N4	90.5(5)	87.9(4)
N3–Pt2–N4	98.5(5)	100.5(4)
Dihedral Angle (°)		
A–B (Pt1)	54.186	33.683
A–C (Pt1)	21.097	4.151
B–C (Pt1)	34.923	30.568
A–B (Pt2)	42.270	42.939
A–C (Pt2)	7.740	13.415
B–C (Pt2)	34.536	29.624

3.3. Absorption and emission spectra

The UV-vis absorption and emission spectra (−)-**1** in CH_2Cl_2 are revealed in Figures 2 and 3. The strong, high-energy absorption bands of complexes (−)-**1** below 330 nm with ε exceeding 10^4 L $mol^{-1}\cdot cm^{-1}$ are ascribed to ligand-centered (LC) $^1\pi$-π^* transitions. The moderately intense bands at a longer wavelength of 350–440 nm ($\varepsilon > 10^3$ L $mol^{-1}\cdot cm^{-1}$) are mainly identified as ^{1}ILCT (intraligand charge transfer) and ^{1}MLCT (metal-to-ligand charge transfer) [40, 41, 42, 43, 44, 45, 46, 47, 48]. In contrast, relatively intense bands at a longer wavelength in Pt(IV) complex (−)-**2** are negligible (Figure S7), which is attributed to the absence of ^{1}MLCT transitions in high valence state Pt(IV) complexes [62, 63].

The CH_2Cl_2 solution of complex (−)-**1** is highly emissive, dominated by a green phosphorescence in the 475–650 nm (Figure 3). The emission maximum is 501 nm, accompanied by a shoulder peak at 530 nm at low

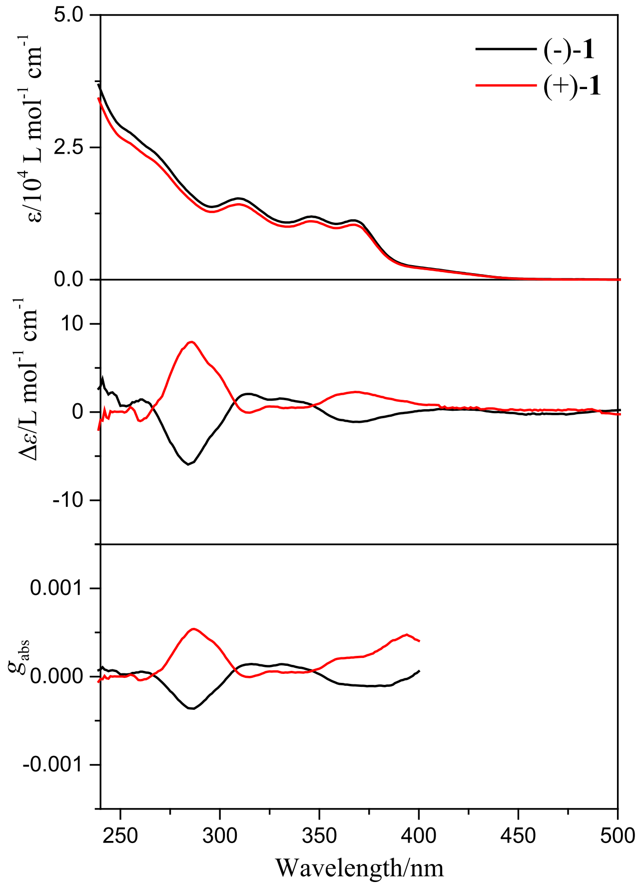

Figure 2. Absorption spectra of (−)-**1** and (+)-**1** in CH_2Cl_2 (5×10^{-5} mol L^{-1}) at T = 298 K; ECD spectra of (−)-**1** and (+)-**1** in CH_2Cl_2 (5×10^{-5} mol L^{-1}) at T = 298 K (middle); g_{abs} factors of (−)-**1** and (+)-**1** (bottom).

concentrations (<5000 μM). According to the reported studies [40, 41, 42, 43, 44, 45, 46, 47, 48], the emission arises mostly from a ^{3}LC ($^3\pi,\pi$) state mixed with some ^{3}MLCT characters. The peak at 501 nm mainly derives from the ^{3}LC state ($^3\pi,\pi$) state, and the peak at 530 nm involves some ^{3}MLCT characters. Further increasing the concentration, the shoulder peak evolves to the emission maximum. However, a lower energy emission corresponding to ^{3}MMLCT or excimer emissive state could not be detected at high concentrations. By examining the crystal structure, none of the effective intermolecular Pt⋯Pt and $\pi-\pi$ interactions are involved in (−)-**1**, and any molecular aggregates could not form. Therefore, the emission is almost concentration-independent. Upon increasing concentration, we tentatively figured out that molecular conformations would vary in concentrated solutions. The geometry would change to maximize the conjugation of 5/6/6 metallocycles, leading to more charge-transfer (CT) character involvement in the emissive state [64]. Accordingly, the emission maximum is bathochromically shifted to 530 nm at high concentrations.

Solvent effects on the absorption and emission of (−)-**1** are also examined (Figure S8). The lowest-energy absorption band is hypsochromically shifted with the increased polarity of the solvents, from 381 nm in toluene to 360 nm in methanol, verifying the character of a CT transition [65, 66, 67]. However, only minimal change (Δλ = 5 nm) of emission maximum can be perceived upon variation of the solvent polarity. The insignificant shift of emission spectra supports the origin of the lowest triplet state from a predominant ^{3}LC state with limited ^{3}MLCT characters [40, 41, 42, 43]. In addition, the solid-state emission spectrum of (−)-**1** shows the maximum at 537 nm and two shoulders at 509 and 569 nm (Figure S9).

3.4. Theoretical investigation

Time-dependent density functional theory (TD-DFT) calculations have been performed to interpret the nature of the transitions [35, 40, 44, 45, 46]. The calculated S_0 geometry of (−)-**1** agrees well with the one determined by the X-ray crystallography, showing a significant distortion from square planarity with a large dihedral angle (37.09°) between the terminal pyridine planes (Figure S10). The optimized S_0 geometry of (−)-**2** exhibits a distorted octahedral geometry, and the tetradentate ligand is curved, which is also comparable to the results in the crystal structure (Table 1).

As depicted in Table S2, the lowest-energy absorption of (−)-**1** mainly derives from the $S_0 \rightarrow S_1$ transition involving HOMO→LUMO (93.0%) and HOMO-2→LUMO (4.5%). According to molecular orbital (MO) patterns and orbital composition analysis (Figure 4 and Table S2), the HOMO is delocalized on the benzene ring of phenyl-pyridine (**Ring D**), benzene ring of phenoxyl-pyridine (**Ring E**), and bridging O atom between phenyl-pyridine and phenoxyl-pyridine, and the rest on central Pt atom (24.02%). In contrast, the LUMO is spread over phenyl-pyridine (**Ring A** and **Ring D**), the pyridine ring of phenoxyl-pyridine (**Ring B**), and the Pt nucleus (6.11%).

For high valence state Pt(IV) complex (−)-**2**, the lowest-energy absorption at 330 nm comes from the $S_0 \rightarrow S_6$ transition concerning HOMO→LUMO+1 (94.3%) and HOMO-1→LUMO+1 (2.43%). The HOMO of (−)-**2** is mainly distributed on the benzene ring of phenyl-pyridine (**Ring D**), benzene ring of phenoxyl-pyridine (**Ring E**), and bridging O atom between phenyl-pyridine and phenoxyl-pyridine, resembling the one of (−)-**1**. The phenyl-pyridine moiety (**Ring A** and **Ring D**) gives a dominant contribution (>90%) to the LUMO+1 of (−)-**2**. Therefore, mixed ^{1}ILCT (tetradentate ligand) and ^{1}MLCT (from Pt(II) atom to tetradentate ligand) transitions should be responsible for the lowest-energy absorption band in the UV-Vis spectrum of (−)-**1**. In contrast, only ^{1}ILCT transitions establish the lowest-energy absorption of (−)-**2**.

Natural transition orbital (NTO) analysis has been executed to investigate the $S_0 \rightarrow T_1$ excitation based on optimized T_1 geometry [44, 45, 46]. As shown in Figure 5 and Table S3, both hole (H) and particle (P) orbitals are resident in phenyl-pyridine moiety (**Ring A** and **Ring D**). In addition, the central Pt atom holds some distributions of both H and P orbitals. Accordingly, it is confirmed that the luminescence of (−)-**1** is ascribed to a primarily ligand-centered (LC) triplet state ($^3\pi,\pi^*$) with some ^{3}MLCT (from Pt(II) atom to phenyl-pyridine moiety) admixture.

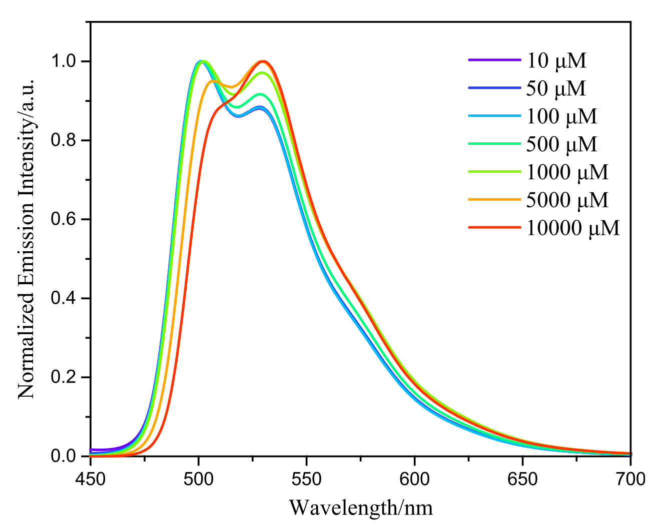

Figure 3. Emission spectra of complex (−)-**1** in CH_2Cl_2 with different concentrations (λ_{ex} = 420 nm).

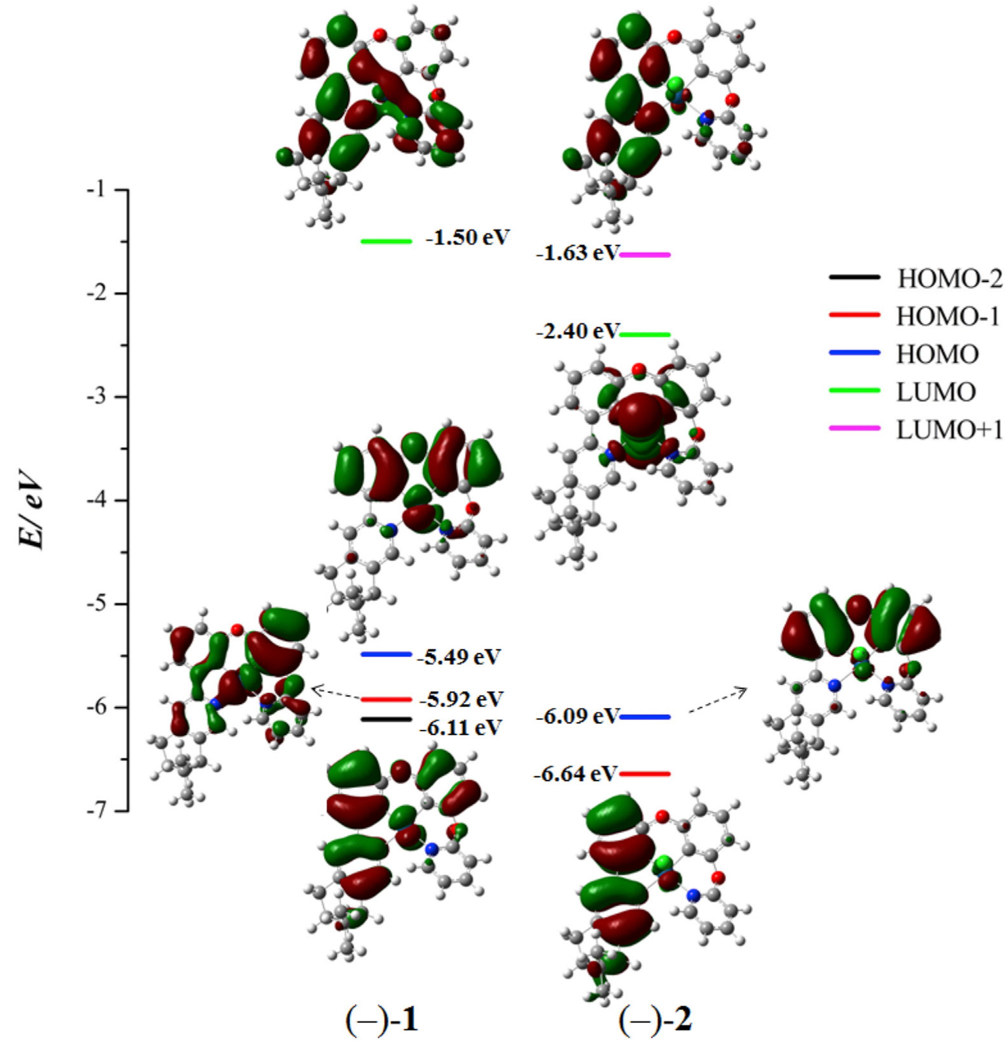

Figure 4. Molecular orbital (MO) patterns of (–)-**1** and (–)-**2** on the basis of their optimized S_0 geometries.

3.5. AIEE properties

Because of solvatochromic behaviors of tetradentate phosphorescent Pt(II) complexes in the solid-state, MacLachlan et al. investigated solvent- and temperature-induced change of emissions in mixed DMSO/water solvents [62]. The continuous addition of water into the DMSO solution of tetradentate phosphorescent Pt(II) complexes caused a transformation from monomeric green emission to excimeric orange emission. Herein, we imagine whether this emission variation exists in pinene-modified tetradentate Pt(II) complex (−)-**1**. However, we failed to observe the change of luminescence from green to orange due to the impossible Pt⋯Pt interactions between neighboring molecules.

Notably, the luminescence of the DMSO solution of (−)-**1** is negligible with Φ_{em} below 1% (Figure 6 and Figure S11). Improving the water content (f_w) from 0 to 40%, we find that the emission intensity has a progressive rise with Φ_{em} attaining 15.92% at f_w = 40%, concomitantly the emission outline stays unchanged with λ_{em} at 501 nm and a shoulder peak at 530 nm, emitting light in green color. Once the proportion of water in DMSO attained 50%, the shoulder peak at 530 nm in pure DMSO solution evolves to the maximum. The solution luminescence appears yellow under UV radiation. Significantly, the emission is intensified sharply, with Φ_{em} reaching the maximum (73.2 %) at f_w = 70%, demonstrating a distinct aggregation-induced emission enhancement (AIEE) behavior.

As a six-membered metallacycle is more flexible than a five-membered metallacycle, the aromatic planes forming the six-membered metallacycle undergo a vibration up and down supported by the big dihedral angles in the crystal structure (Table 1), which would favor non-radiative decay, inducing relatively weak emissions [64]. In pure DMSO solution, the non-radiative vibration is continual, leading to an extremely low Φ_{em}. Continuous addition of water to the DMSO solution causes the formation of aggregates. On the basis of the RIR and RIV mechanisms, the intramolecular vibration and rotation can be efficiently suppressed in aggregates, restraining non-radiative decay and promoting radiative decay processes [68, 69, 70]. When the water content increases to a critical value of 50%, many aggregates form in a mixed solution, resulting in a dramatic increase in emission intensity. Concurrently, the geometrical change to maximize conjugation of 5/6/6 metallocycles occurs in the aggregates, leading to more ^{3}MLCT transitions in the emissive state [64, 71]. Consequently, the shoulder peak at 530 nm develops to the emission maximum.

3.6. Chiroptical properties

Electronic circular dichroism (ECD) and circularly polarized luminescence (CPL) spectra have been recorded to explore the chiroptical properties of (−)-**1**, (+)-**1** (−)-**2**, and (+)-**2** (Figures 2 and 7). Complex (−)-**1** presents two negative Cotton effects at 290 and 390 nm with absorption dissymmetry ratio $|g_{abs}|$ 5 × 10^{-4} and 4 × 10^{-4}. In addition, a weak positive Cotton effect at 310 nm can be recognized. Meanwhile, the enantiomer (+)-**1** shows approximately opposite signals with a

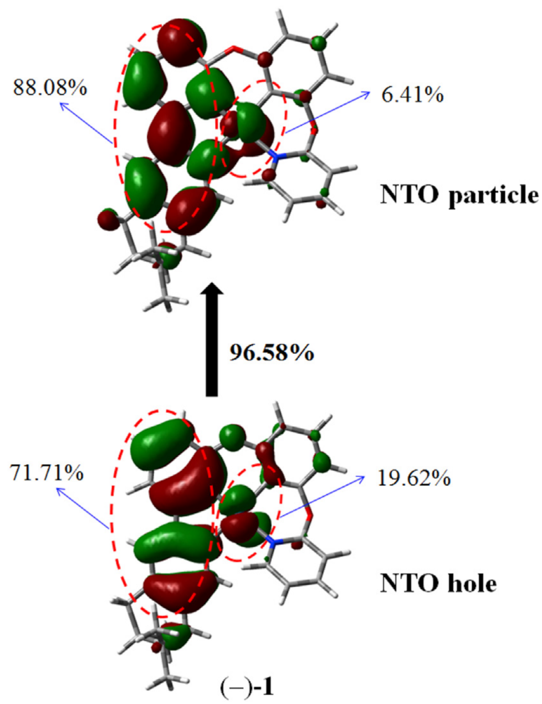

Figure 5. Natural transition orbital pattern for S_0-T_1 excitation of (–)-**1** on the basis of its optimized T_1 geometry.

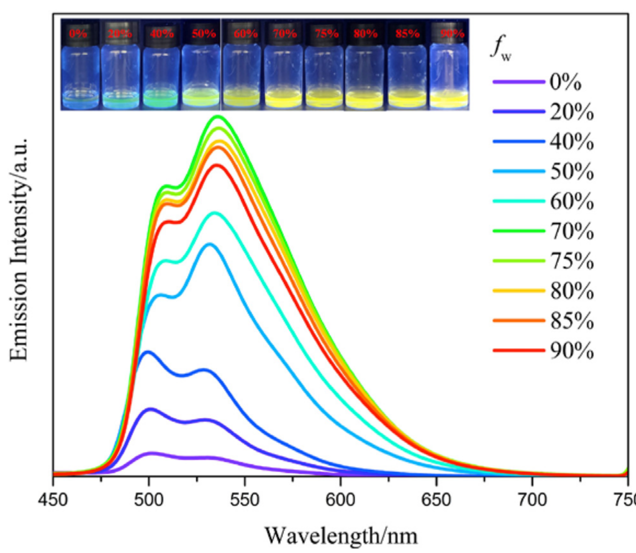

Figure 6. Emission spectra (λ_{ex} = 420 nm) of (–)-**1** (5 × 10^{-5} mol L^{-1}) in DMSO/water mixed solvent. Inset page: the luminescent photos of (–)-**1** (5 × 10^{-5} mol L^{-1}) in DMSO/water mixed solvent under irradiation with 365 nm light.

comparable magnitude of $|g_{abs}|$ at the same wavelengths. A series of negative Cotton effects in the region of 280–330 nm and a positive Cotton effect at 255 nm are observed for (−)-**2**. A mirror-symmetric ECD spectrum is revealed for the enantiomer (+)-**2**. No Cotton effects originating from ^{1}MLCT processes are found above 350 nm for Pt(IV) complexes (−)-**2** and (+)-**2** [62-63].

As tetradentate Pt(II) enantiomer (−)-**1** is strongly emissive and exhibits a platinum centroid helix chirality, we further measure its CPL activity. Complexes (−)-**1** and (+)-**1** show symmetrically appreciable

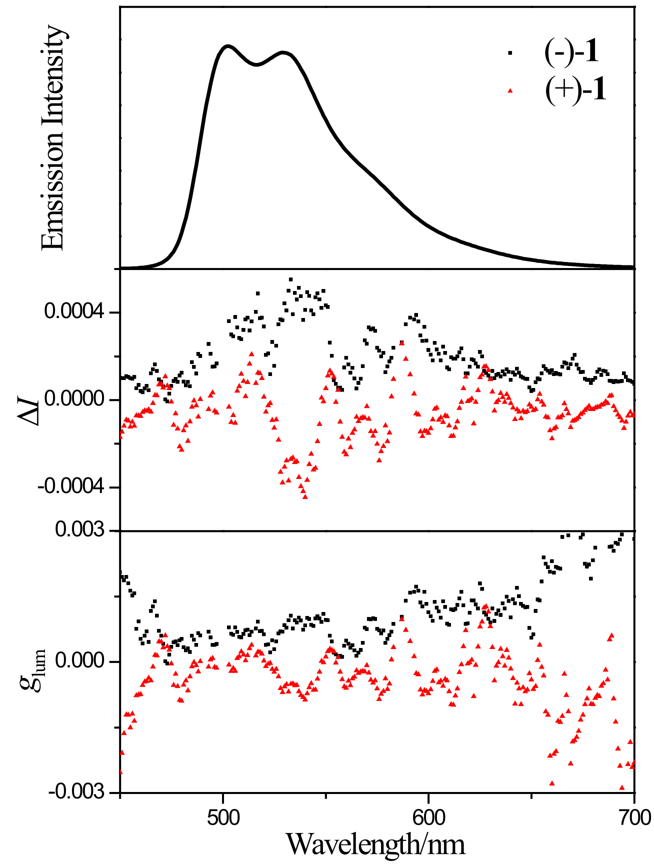

Figure 7. Emission, CPL and g_{lum} spectra of (−)-**1** and (+)-**1** in CH_2Cl_2 solution at RT (10^{-3} mol L^{-1}).

CPL signals at 480–620 nm with the g_{lum} factors on the order of 10^{-3} (+1.05 × 10^{-3} for (−)-**1** and -0.93 × 10^{-3} for (+)-**1** at 530 nm) (Figure 7). The dissymmetric factor is comparable to the CPL signals for the reported phosphorescent CPL-active Pt(II) complexes with helicene, axial chirality, helical chirality, and chiral-at-metal [7, 8, 9, 10, 11, 12, 13, 14, 15, 16, 17, 18, 19, 20, 21, 22, 23, 24, 25, 26, 27, 28, 29, 30, 31].

4. Conclusion

In summary, two valence forms of tetradentate platinum complexes, Pt(II) enantiomers ((−)-**1** and (+)-**1**) and tetradentate Pt(IV) enantiomers ((−)-**2** and (+)-**2**), have been prepared and characterized. Fused 5/6/6 metallocycles are generated after tetradentate coordination. The solution and solid of (−)-**1** are strongly emissive, whereas the luminescence of (−)-**2** is silent. The emission of (−)-**1** is mainly ascribed to a ^{3}LC state ($^3\pi,\pi$) mixed with some ^{3}MLCT characters, further verified by the NTO analysis. The DMSO/water solution of (−)-**1** demonstrates a distinct aggregation-induced emission enhancement (AIEE) behavior, with emission quantum yield (Φ_{em}) intensifying sharply upon increasing the water content. In addition, the continuous addition of water to the DMSO solution causes a geometrical change to maximize the conjugation of 5/6/6 metallocycles, leading to more ^{3}MLCT transitions in the emissive state. Benefiting a distorted square-planar geometry and a platinum centroid helix chirality of (−)-**1** as revealed in the structure, symmetrically distinct CPL activities with the glum factors on the order of 10^{-3} (+1.05 × 10^{-3} for (−)-**1** and -0.93 × 10^{-3} for (+)-**1** at 530 nm) have been observed for highly phosphorescent Pt(II) enantiomers. This work provides a strategy for developing multi-dentate coordinated CPL-active complexes based on chiral-at-metal.

Declarations

Author contribution statement

Hua-Hong Zhang: Performed the experiments; Analyzed and interpreted the data; Contributed reagents, materials, analysis tools or data; Wrote the paper.

Jing Jing: Performed the experiments; Contributed reagents, materials, analysis tools or data.

Guo Xu: Performed the experiments; Analyzed and interpreted the data.

Yi-Xin Song: Performed the experiments.

Shui-Xing Wu, Zai-Feng Shi: Analyzed and interpreted the data.

Xing-Han Chen, Da-Shuai Zhang: Contributed reagents, materials, analysis tools or data.

Xiao-Peng Zhang: Conceived and designed the experiments; Analyzed and interpreted the data; Wrote the paper.

Funding statement

This work is supported by the National Natural Science Foundation of China (No. 21961009) and the Natural Science Foundation of Hainan Province (No. 220RC591).

Data availability statement

Data included in article/supplementary material/referenced in article.

Declaration of interests statement

The authors declare no conflict of interest.

Additional information

Supplementary content related to this article has been published online at https://doi.org/10.1016/j.heliyon.2022.e11358.

References

[1] J.R. Brandt, X. Wang, Y. Yang, A.J. Campbell, M.J. Fuchter, Circularly polarized phosphorescent electroluminescence with a high dissymmetry factor from PHOLEDs based on a platinahelicene, J. Am. Chem. Soc. 138 (2016) 9743–9746.
[2] Z.-P. Yan, X.-F. Luo, W.-Q. Liu, Z.-G. Wu, X. Liang, K. Liao, Y. Wang, Y.-X. Zheng, L. Zhou, J.-L. Zuo, Y. Pan, H. Zhang, Configurationally stable platinahelicene enantiomers for efficient circularly polarized phosphorescent organic light-emitting diodes, Chem. Eur J. 25 (2019) 5672–5676.
[3] G. Qian, X. Yang, X. Wang, J.D. Herod, D.W. Bruce, S. Wang, W. Zhu, P. Duan, Y. Wang, Chiral platinum-based metallomesogens with highly efficient circularly polarized electroluminescence in solution-processed organic light-emitting diodes, Adv. Opt. Mater. 8 (2020), 2000775.
[4] Z. Jiang, J. Wang, T. Gao, J. Ma, Z. Liu, R. Chen, Rational design of axially chiral platinabinaphthalenes with aggregation-induced emission for red circularly polarized phosphorescent organic light-emitting diodes, ACS Appl. Mater. Interfaces 12 (2020) 9520–9527.
[5] L. Wang, H. Xiao, L. Qu, J. Song, W. Zhou, X. Zhou, H. Xiang, Z.-X. Xu, Axially chiral bis-cycloplatinated binaphthalenes and octahydro binaphthalenes for efficient circularly polarized phosphorescence in solution-processed organic light-emitting diodes, Inorg. Chem. 60 (2021) 13557–13566.
[6] T. Biet, T. Cauchy, Q. Sun, J. Ding, A. Hauser, P. Oulevey, T. Bürgi, D. Jacquemin, N. Vanthuyne, J. Crassous, N. Avarvari, Triplet state CPL active helicene-dithiolene platinum bipyridine complexes, Chem. Commun. 53 (2017) 9210–9213.
[7] C. Shen, E. Anger, M. Srebro, N. Vanthuyne, K.K. Deol, T.D. Jefferson Jr., G. Muller, J.A.G. Williams, L. Toupet, C. Roussel, J. Autschbach, R. Réau, J. Crassous, Straightforward access to mono- and bis-cycloplatinated helicenes that display circularly polarized phosphorescence using crystallization resolution methods, Chem. Sci. 5 (2014) 1915–1927.
[8] P. Vázquez-Domínguez, O. Journaud, N. Vanthuyne D. Jacquemin, L. Favereau, J. Crassous, A. Ros, Helical donor-acceptor platinum complexes displaying dual luminescence and near-infrared circularly polarized luminescence, Dalton Trans. 50 (2021) 13220–13226.
[9] J. Song, M. Wang, X. Xu, L. Qu, X. Zhou, H. Xiang, 1D-helical platinum(II) complexes bearing metal induced chirality, aggregation-induced red phosphorescence and circularly polarized luminescence, Dalton Trans. 48 (2019) 4420–4428.
[10] R. Inoue, R. Kondo, Y. Morisaki, Experimental and theoretical studies on circularly polarized phosphorescence of a [2.2]paracyclophane-based platinum(II) complex, Chem. Commun. 56 (2020) 15438–15441.
[11] T. Ikeda, M. Takayama, J. Kumar, T. Kawai, T. Haino, Novel helical assembly of a Pt(II) phenylbipyridine complex directed by metal–metal interaction and aggregation-induced circularly polarized emission, Dalton Trans. 44 (2015) 13156–13162.
[12] T. Ikeda, K. Hirano, T. Haino, Circularly polarized luminescent organogel based on Pt(II) complex possessing phenylisoxazoles, Mater. Chem. Front. 2 (2018) 468–474.
[13] G. Park, H. Kim, H. Yang, K.R. Park, I. Song, J.H. Oh, C. Kim, Y. You, Amplified circularly polarized phosphorescence from co-assemblies of platinum(II) complexes, Chem. Sci. 10 (2019) 1294–1301.
[14] S. Lee, Y. Lee, K. Kim, S. Heo, D.Y. Jeong, S. Kim, J. Cho, C. Kim, Y. You, Twist to boost: circumventing quantum yield and dissymmetry factor trade-off in circularly polarized luminescence, Inorg. Chem. 60 (2021) 7738–7752.
[15] Z.-L. Gong, Y.-W. Zhong, Handedness-inverted polymorphic helical assembly and circularly polarized luminescence of chiral platinum complexes, Sci. China Chem. 64 (2021) 788–799.
[16] B. Li, Y. Li, M.H.-Y. Chan, V.W.-W. Yam, Phosphorescent cyclometalated platinum(II) enantiomers with circularly polarized luminescence properties and their assembly behaviors, J. Am. Chem. Soc. 143 (2021) 21676–21684.
[17] G.-F. Huo, Q. Tu, Y.-X. Hu, B. Jiang, Q.-F. Zhou, Y. Niu, X. Zhao, H.-M. Ding, J. Wen, G.-Q. Yin, X. Shi, L. Xu, Amplified circularly polarized luminescence promoted by hierarchical selfassembly involving Pt⋯Pt interactions, Sci. China Mater. 65 (2022) 469–476.
[18] Z.-L. Gong, T.-X. Dan, J. Yao, Y.-W. Zhong, Supramolecular assembly and circularly polarized phosphorescence of tridentate platinum-isocyanide complexes modified with a chiral leucine derivative, Chem. Photo Chem. 6 (2022), e202100239.
[19] S.G. Kang, K.Y. Kim, Y. Cho, D.Y. Jeong, J.H. Lee, T. Nishimura, S.S. Lee, S.K. Kwak, Y. You, J.H. Jung, Circularly polarized luminescence active supramolecular nanotubes based on Pt(II) complexes that undergo dynamic morphological transformation and helicity inversion, Angew. Chem. Int. Ed. 61 (2022), e202207310.
[20] T.R. Schulte, J.J. Holstein, L. Krause, R. Michel, D. Stalke, E. Sakuda, K. Umakoshi, G. Longhi, S. Abbate, G.H. Clever, Chiral-at-Metal phosphorescent square-planar Pt(II)- complexes from an achiral organometallic ligand, J. Am. Chem. Soc. 139 (2017) 6863–6866.
[21] H. Zhu, Q. Li, B. Shi, H. Xing, Y. Sun, S. Lu, L. Shangguan, X. Li, F. Huang, P.J. Stang, formation of planar chiral platinum triangles via pillar[5]arene for circularly polarized luminescence, J. Am. Chem. Soc. 142 (2020) 17340–17345.
[22] B. Yang, G. Zou, S. Zhang, H. Ni, H. Wang, W. Xu, C. Yang, H. Zhang, W. Yu, K. Luo, Biased symmetry breaking and chiral control by self-replicating in achiral tetradentate platinum (II) complexes, Angew. Chem. Int. Ed. 60 (2021) 10531–10536.
[23] S. Horiuchi, S. Moon, A. Ito, J. Tessarolo, E. Sakuda, Y. Arikawa, G.H. Clever, K. Umakoshi, Multinuclear Ag clusters sandwiched by Pt complex units: fluxional behavior and chiral-at-cluster photoluminescence multinuclear Ag clusters sandwiched by Pt complex units: fluxional behavior and chiral-at-cluster photoluminescence, Angew. Chem. Int. Ed. 60 (2021) 10654–10660.
[24] T. Usuki, H. Uchida, K. Omoto, Y. Yamanoi, A. Yamada, M. Iwamura, K. Nozaki, H. Nishihara, Enhancement of photofunction of phosphorescent Pt(II) cyclometalated complexes driven by substituents: solid state luminescence and circularly polarized luminescence, J. Org. Chem. 84 (2019) 10749–10756.
[25] B. Yang, H. Ni, H. Wang, Y. Hu, K. Luo, W. Yu, Enhanced synchronously emission dissymmetry factor and quantum efficiency of circularly polarized phosphorescence from point-chiral cyclometalated platinum(II) liquid crystal, J. Phys. Chem. C 124 (2020) 23879–23887.
[26] W. Hagui, M. Cordier, J. Boixel, J.-F. Soulé, Access to functionalized luminescent Pt(II) complexes by photoredox-catalyzed Minisci alkylation of 6-aryl-2,2'-bipyridines, Chem. Commun. 57 (2021) 1038–1041.
[27] J. Song, H. Xiao, L. Fang, L. Qu, X. Zhou, Z.-X. Xu, C. Yang, H. Xiang, Highly phosphorescent planar chirality by bridging two square planar platinum(II) complexes: chirality induction and circularly polarized luminescence, J. Am. Chem. Soc. 144 (2022) 2233–2244.
[28] L. Yuan, Q.-J. Ding, Z.-L. Tu, X.-J. Liao, X.-F. Luo, Z.-P. Yan, Z.-G. Wu, Y.-X. Zheng, Molecular self-induced configuration for improving dissymmetry factors in tetradentate platinum(II) enantiomers cycloaddition, Chin. Chem. Lett. 33 (2022) 1459–1462.
[29] M. Ikeshita, S. Furukawa, T. Ishikawa, K. Matsudaira, Y. Imai, T. Tsuno, Enhancement of chiroptical responses of trans-Bis[(β-iminomethyl)naphthoxy] platinum(II) complexes with distorted square planar coordination geometry, ChemistryOpen 11 (2022), e202100277.
[30] G. Fu, Y. He, W. Li, B. Wang, X. Lu, H. He, W.-Y. Wong, Efficient polymer light-emitting diodes (PLEDs) based on chiral [Pt(CN)(NO)] complexes with near-infrared (NIR) luminescence and circularly polarized (CP) light, J. Mater. Chem. C 7 (2019) 13743–13747.
[31] L. Yuan, T.-T. Liu, M.-X. Mao, X.-F. Luo, Y.-X. Zheng, Configurationally stable helical tetradentate Pt(II) complexes for organic light-emitting diodes with circularly polarized electroluminescence, J. Mater. Chem. C 9 (2021) 14669–14674.
[32] G. Li, Q. Chen, J. Zheng, Q. Wang, F. Zhan, W. Lou, Y.-F. Yang, Y. She, Metal-assisted delayed fluorescent Pd(II) complexes and phosphorescent Pt(II) complex based on [1,2,4]Triazolo[4,3-*a*]pyridine-Containing ligands: Synthesis,

characterization, electrochemistry, photophysical studies, and application, Inorg. Chem. 58 (2019) 14349–14360.
[33] G. Cheng, Y. Kwak, W.-P. To, T.L. Lam, G.S.M. Tong, M.K. Sit, S. Gong, B. Choi, W.i. Choi, C. Yang, C.-M. Che, High efficiency solution-processed organic light-emitting diodes with tetradentate platinum(II) emitters, ACS Appl. Mater. Interfaces 11 (2019) 45161–45170.
[34] H. Ma, K. Shen, Y. Wu, F. Xia, F. Yu, Z. Sun, C. Qian, Q. Peng, H.-H. Zhang, C. You, G. Xie, X.-C. Hang, W. Huang, High-color-purity and efficient solution-processable blue phosphorescent light-emitting diodes with Pt(II) complexes featuring $^3\pi\pi^*$ transition, Mater. Chem. Front. 3 (2019) 2448–2454.
[35] T. Fleetham, J.H. Golden, M. Idris, H.-M. Hau, D.S.M. Ravinson, P.I. Djurovich, M.E. Thompson, Tuning state energies for narrow blue emission in tetradentate pyridyl-carbazole platinum complexes, Inorg. Chem. 58 (2019) 12348–12357.
[36] J.-S. Huh, M.J. Sung, S.-K. Kwon, Y.-H. Kim, J.-J. Kim, Highly efficient deep blue phosphorescent OLEDs based on tetradentate Pt(II) complexes containing adamantyl spacer groups, Adv. Funct. Mater. 31 (2021), 2100967.
[37] D. Wu, K. Qin, X. Gao, S. Cheng, A. Wu, C. Sha, H. Ma, Z. Sun, C. Zhang, X.-C. Hang, Color-tuning Pt(II) complexes for natural-light electrophosphorescence, J. Mater. Chem. C 10 (2022) 1365.
[38] Y. She, K. Xu, X. Fang, Y.-F. Yang, W. Lou, Y. Hu, Q. Zhang, G. Li, Tetradentate platinum(II) and palladium(II) complexes containing fused 6/6/6 or 6/6/5 metallocycles with azacarbazolylcarbazole-based ligands, Inorg. Chem. 60 (2021) 12972–12983.
[39] I. Maisuls, C. Wang, M.E.G. Suburu, S. Wilde, C.-G. Daniliuc, D. Brunink, N.L. Doltsinis, S. Ostendorp, G. Wilde, J. Kosters, U. Resch-Genger, C.A. Strassert, Ligand-controlled and nanoconfinement-boosted luminescence employing Pt(II) and Pd(II) complexes: from color-tunable aggregation-enhanced dual emitters towards self-referenced oxygen reporters, Chem. Sci. 12 (2021) 3270–3281.
[40] G. Li, H. Guo, X. Fang, Y.-F. Yang, Y. Sun, W. Lou, Q. Zhang, Y. She, Tuning the excited state of tetradentate Pd(II) and Pt(II) complexes through benzannulated N-heteroaromatic ring and central metal, Chin. J. Chem. 40 (2022) 223–234.
[41] E. Turner, N. Bakken, J. Li, Cyclometalated platinum complexes with luminescent quantum yields approaching 100, Inorg. Chem. 52 (2013) 7344–7351.
[42] G. Li, X. Zhao, T. Fleetham, Q. Chen, F. Zhan, J. Zheng, Y.F. Yang, W. Lou, Y. Yang, K. Fang, Z. Shao, Q. Zhang, Y. She, Tetradentate platinum(II) complexes for highly efficient phosphorescent emitters and sky blue OLEDs, Chem. Mater. 32 (2020) 537–548.
[43] C. You, F. Xia, Y. Zhao, Y. Zhang, Y. Sheng, Y. Wu, X.-C. Hang, F. Chen, H. Ma, K. Shen, Z. Sun, T. Ueba, S. Kera, C. Zhang, H. Zhang, Z.-K. Chen, W. Huang, Probing triplet excited states and managing blue light emission of neutral tetradentate platinum(II) complexes, J. Phys. Chem. Lett. 9 (2018) 2285–2292.
[44] L. Zhu, C. Sha, A. Lv, W. Xie, K. Shen, Y. Chen, G. Xie, H. Ma, H. Li, X.-C. Hang, Tetradentate Pt(II) complexes with peripheral hindrances for highly efficient solution-processed blue phosphorescent OLEDs, Inorg. Chem. 61 (2022) 10402–10409.
[45] Y. Wu, X. Tan, A. Lv, F. Yu, H. Ma, K. Shen, Z. Sun, F. Chen, Z.-K. Chen, X.-C. Hang, Triplet excited-state engineering of phosphorescent Pt(II) complexes, J. Phys. Chem. Lett. 10 (2019) 5105–5110.
[46] G. Li, F. Zhan, J. Zheng, Y.-F. Yang, Q. Wang, Q. Chen, G. Shen, Y. She, Highly efficient phosphorescent tetradentate platinum(II) complexes containing fused 6/5/6 metallocycles, Inorg. Chem. 59 (2020) 3718–3729.
[47] C. Lee, R. Zaen, K.-M. Park, K.H. Lee, J.Y. Lee, Y. Kang, Blue phosphorescent platinum complexes based on tetradentate bipyridine ligands and their application to organic light-emitting diodes (OLEDs), Organometallics 37 (2018) 4639–4647.
[48] L. Zhu, W. Xie, C. Qian, W. Xie, K. Shen, A. Lv, H. Ma, H. Li, X.-C. Hang, W. Li, S.-J. Su, W. Huang, Tetradentate Pt(II) complexes for spectrum-stable deep-blue and white electroluminescence, Adv. Opt. Mater. 8 (2020), 2000406.
[49] W. Liu, L. Zhou, L.Y. Jin, W. Xie, C.-M. Che, G. Cheng, Improved color quality in double-EML WOLEDs by using a tetradentate Pt(II) complex as a green/red emitter, J. Mater. Chem. C 9 (2021) 3384–3390.
[50] X.-P. Zhang, V.Y. Chang, J. Liu, W. Huang, Y.-Z. Li, C.-H. Li, G. Muller, X.-Z. You, Potential switchable circularly polarized luminescence from chiral cyclometalated platinum(II) complexes, Inorg. Chem. 54 (2015) 143–152.
[51] X.-P. Zhang, L.-L. Wang, X.-W. Qi, D.-S. Zhang, Q.-Y. Yang, Z.-F. Shi, Q. Lin, T. Wu, Pt···Pt interaction triggered tuning of circularly polarized luminescence activity in chiral dinuclear platinum(II) complexes, Dalton Trans. 47 (2018) 10179–10186.
[52] Q.-Y. Yang, H.-H. Zhang, X.-L. Han, S.-D. Weng, Y. Chen, J.-L. Wu, L.-Z. Han, X.-P. Zhang, Z.-F. Shi, Enhanced circularly polarized luminescence activity in chiral platinum(II) complexes with bis- or triphenylphosphine ligands, Front. Chem. 8 (2020) 303.
[53] H.-H. Zhang, J. Jing, S.-X. Wu, Y.-P. Luo, S.-S. Sun, D.-S. Zhang, Z.-F. Shi, X.-P. Zhang, Tunable circularly polarized luminescence of sol-gels based on chiral cyclometalated platinum(II) complexes, Dyes Pigments 201 (2022), 110228.
[54] J. Jing, G. Xu, H.-H. Zhang, X.-H. Chen, D.-S. Zhang, L.-Z. Han, X.-W. Qi, Z.-F. Shi, X.-P. Zhang, Enhanced circularly polarized luminescence in fluoro-substituted NCN-coordinating platinum(II) complexes, Inorg. Chim. Acta. 541 (2022), 121067.
[55] S. Tanaka, K. Sato, K. Ichida, T. Abe, T. Tsubomura, T. Suzuki, K. Shinozaki, Circularly polarized luminescence of chiral Pt(pppb)Cl (pppbH=1-pyridyl-3-(4,5-pinenopyridyl)benzene) aggregate in the excited state, Chem. Asian J. 11 (2016) 265–273.
[56] Z. Li, Y. Han, F. Nie, M. Liu, H. Zhong, F. Wang, Bright and robust phosphorescence achieved by non-Covalent clipping, Angew. Chem. Int. Ed. 60 (2021) 8212–8219.
[57] SAINT-plus, Version 6.02, Bruker Analytical X-ray System, Madison, WI, 1999.
[58] G.M. Sheldrick, SADABS, an Empirical Absorption Correction Program, Bruker Analytical X-ray Systems, Madison, WI, 1996.
[59] G.M. Sheldrick, Acta Crystallogr. A64, 2008, p. 112.
[60] M.J. Frisch, Gaussian 09, Revision C.01, Gaussian, Inc., Wallingford, CT, 2009.
[61] T. Lu, F. Chen, Multiwfn: a multifunctional wavefunction analyzer, J. Comput. Chem. 33 (2012) 580–592.
[62] Q.-Y. Yang, H.-H. Zhang, X.-W. Qi, S.-S. Sun, D.-S. Zhang, L.-Z. Han, X.-P. Zhang, Z.-F. Shi, Mechanochromic luminescence properties of fluoro-substituted pinene-containing cyclometalated platinum(II) complexes with multiple triplet excited states, Dalton Trans. 50 (2021) 8938–8946.
[63] M.A. Soto, V. Carta, R.J. Andrews, M.T. Chaudhry, M.J. MacLachlan, Structural elucidation of selective solvatochromism in a responsive-at-metal cyclometalated platinum(II) complex, Angew. Chem. Int. Ed. 59 (2020) 10348–10352.
[64] X.-P. Zhang, F.-Q. Liu, J.-C. Lai, C.-H. Li, A.-M. Li, X.-Z. You, Novel redox responsive chiral cyclometalated platinum(II) complexes with pinene functionalized CNN ligands, New J. Chem. 40 (2016) 2628–2636.
[65] H.-H. Zhang, S.-X. Wu, Y.-Q. Wang, T.-G. Xie, S.-S. Sun, Y.-L. Liu, L.-Z. Han, X.-P. Zhang, Z.-F. Shi, Mechanochromic luminescent property and anti-counterfeiting application of AIE-active cyclometalated platinum(II) complexes featuring a fused five-six-membered metallacycle, Dyes Pigments 197 (2022), 109857.
[66] Z. Ding, H. Chen, Y. Han, P. Gao, J. Liu, Improving electrochromic performance of panchromatic all-in-one devices by retarding interfacial molecular aggregation/degradation in anode electrode, Sol. Energy Mater. Sol. Cell. 246 (2022), 111924.
[67] M. Shu, J. Tao, Y. Han, W. Fu, X. Li, R. Zhang, J. Liu, Molecular engineering of terpyridine-Fe(II) coordination polymers consisting of quinoxaline-based π-spacers toward enhanced electrochromic performance, Polymer 256 (2022), 125231.
[68] X. Li, J. Gu, Z. Zhou, W. Liu, J. Gao, Q. Wang, Precise control for the aggregation and deaggregation with the aid of a tetraphenylethylene derivative: luminescence modulation and sensing performance, Dyes Pigments 172 (2020), 107844.
[69] J. Mei, N.L.C. Leung, R.T.K. Kwok, J.W.Y. Lam, B.Z. Tang, Aggregation-induced emission: together we shine, united we soar, Chem. Rev. 115 (2015) 11718–11940.
[70] J. Gu, X. Li, Z. Zhou, R. Liao, J. Gao, Y. Tang, Q. Wang, Synergistic regulation of effective detection for hypochlorite based on a dual-mode probe by employing aggregation induced emission (AIE) and intramolecular charge transfer (ICT) effects, Chem. Eng. J. 368 (2019) 157–164.
[71] X. Yang, L. Yue, Y. Yu, B. Liu, J. Dang, Y. Sun, G. Zhou, Z. Wu, W.-Y. Wong, Strategically formulating aggregation-induced emission-active phosphorescent emitters by restricting the coordination skeletal deformation of Pt(II) complexes containing two independent monodentate ligands, Adv. Opt. Mater. 8 (2020), 2000079.